Int. J. Heat Mass Transfer. Vol. 27, No. 2, pp. 221–231, 1984
Printed in Great Britain

0017-9310/84 $3.00 + 0.00

COMBINED CONVECTION AND RADIATION IN RECTANGULAR DUCTS

K. H. IM and R. K. AHLUWALIA
Engineering Division, Argonne National Laboratory, Bldg. 207, 9700 S. Case Avenue, Argonne, IL 60439, U.S.A.

(*Received* 8 *October* 1982 *and in revised form* 20 *May* 1983)

Abstract—Combined convective and radiative heat transfer in rectangular ducts is analyzed by solving simultaneously the fluid dynamic equations and the radiation transport equation. The major approximations invoked in the analysis are the assumption of parabolic flow for the fluid equations and the use of the moment method for simplifying the radiation transport equation. The analysis is applicable to general compressible, turbulent, developing, radiating flow in rectangular ducts in the presence of scattering particles. In the sample calculations, Mie theory is used for determining the spectral absorption and scattering coefficients of the particles.

NOMENCLATURE

C_1, C_2, C_D	turbulence constants
G	incident radiation
H	height
I	radiation intensity
$\hat{i}, \hat{j}, \hat{k}$	unit vectors in x-, y- and z-directions
K	Green's function
k	kinetic energy of turbulence
l	directional cosine
p	pressure
$\bar{p}$	average pressure
Q	radiative heat flux
q	convective heat flux
T	temperature
u	axial velocity
v, w	velocity in y- and z-directions
W	width
x	flow direction
y, z	transverse directions.

Greek symbols

β	extinction coefficient
κ	scattering coefficient
ν	frequency
μ	viscosity
ρ	density
ε	dissipation rate of k
ε_w	wall emissivity
σ	Prandtl number
τ	shear stress
τ, ξ	optical thicknesses
θ	polar angle
ϕ	azimuthal angle
Ω	solid angle
$\hat{\Omega}$	beam direction.

Subscripts

b	black body
h	enthalpy
k	turbulence kinetic energy
l	laminar
t	turbulent
eff	effective
w	wall
x, y, z	coordinate directions
ν	spectral
ε	dissipation rate of k.

1. INTRODUCTION

IN MANY engineering applications related to energy systems, such as coal, oil or gas-fired furnaces and the components of a coal-fired magnetohydrodynamic plant (channel, diffuser and radiant boiler), the convection and radiation modes of heat transfer are both important. In such applications, the fluid and radiation transport equations must be solved simultaneously in order to determine the heat transfer rate and the system performance. Even in flow applications (e.g. high-temperature MHD combustor) where radiation dominates over convection as the principal heat transfer mechanism, it may still be important to consider turbulent convection because of its role in determining the temperature profile. One of the difficulties in dealing with the combined convection and radiation problem is the large computation time needed for performing spectral calculations. The degree of difficulty increases if there are absorbing and scattering particles present. In such situations, it becomes imperative to seek a simplification of the radiation transport equation. One method of achieving the required simplification is the differential approximation.

In previous publications, coupled convection–radiation solutions were obtained using the P_1 approximation when the system configuration could be approximated as boundary layer flow between infinite parallel plates [1, 2] or in pipes [3]. It has been shown by Krook [4] that the P_1 approximation and the differential approximation (moment method) are entirely synonymous when applied to the radiation transport equation. This study deals with the extension

of the solution method developed in refs. [1–3] to the multi-dimensional problem encountered more often in practice: compressible, turbulent, developing, radiating flow in rectangular ducts in the presence of scattering particles. It has been shown previously by Cheng [5] that under realistic conditions, the accuracy of differential approximation for multi-dimensional problems is comparable to that for one-dimensional (1-D) problems, and that Marshak's boundary condition is more accurate than the Mark's boundary condition for problems in Cartesian coordinate geometries.

The accuracy of the P_1 approximation for rectangular geometry has been assessed by Ratzel and Howell [6] for the hypothetical situation of a square enclosure having gray medium in radiative equilibrium, with three surfaces prescribed zero and the fourth prescribed unity emissive power. For the case of black walls and unity optical thickness, the heat flux and medium emissive power calculated from the P_1 approximation were found to be in error by nearly 20%. For gray surfaces (more common case) having 0.5 surface emissivity, the error decreased to less than 10%. The P_1 approximation became almost exact on further reducing the surface emissivity to 0.1. The P_1 approximation was stated to be more accurate in the optically thick rather than the thin limit. For the realistic case of non-gray gaseous radiation, the inaccuracy of the P_1 approximation in the optically thin limit may not be a serious limitation. This is because the maximum emission and absorption of radiation occurs near the band center, and the medium is optically thick at these frequencies. Also, for combustion problems the inaccuracies cited in ref. [6] should be regarded as upper bounds because of the use of (1) the radiative equilibrium assumption implying a jump in medium emissive power at the wall, and (2) discontinuous boundary condition at the corner. For the problem of combined convective–radiative heat transfer in combustors, these discontinuities will not be present. It appears feasible to improve the accuracy of the P_1 approximation with the use of the modification proposed by Modest [7] but this has not been attempted in the present work.

In the flow model of this study, the particles are assumed to be locally in thermal equilibrium and near velocity equilibrium with the gas. For the sub-micrometer size particles considered, these are regarded as reasonable assumptions. Other approximations imposed on the analytical model are listed in Sections 2–4. A significant assumption is the approximation of no flow recirculation in the axial direction. As a direction for future research, the need to develop a faster algorithm for solving the finite-difference equations resulting from the discretization of the radiation transport equation has become apparent. In the sample calculations presented, carbon dioxide, water vapor and particles are considered as the major participating species. The spectral absorption coefficients of the gaseous species are determined from a band model. For the particles, Mie theory is employed for calculating the spectral absorption and scattering coefficients.

2. GOVERNING EQUATIONS

In the present study, flow and thermal fields in the duct are simulated through the parabolic form of the three-dimensional (3-D) compressible, turbulent Navier–Stokes equations. The key assumptions of the flow and heat transfer model are given below.

(1) Axial diffusion of flow and heat is negligible in comparison to the diffusion in transverse directions. This assumption is well-suited for flows with no axial recirculation.

(2) For numerical purposes, longitudinal and lateral pressure gradients are assumed to be uncoupled. This assumption is nearly satisfied when the flow is predominantly axial so that no significant lateral pressure gradients can exist.

Under the above assumptions, the governing equations reduce to the following set.

2.1. *Continuity*

$$\frac{\partial}{\partial x}(\rho u)+\frac{\partial}{\partial y}(\rho v)+\frac{\partial}{\partial z}(\rho w)=0. \tag{1}$$

2.2. *Momentum*

$$\frac{\partial}{\partial x}(\rho uu)+\frac{\partial}{\partial y}(\rho vu)+\frac{\partial}{\partial z}(\rho wu)=-\frac{\partial \bar{p}}{\partial x}+\frac{\partial \tau_{xy}}{\partial y}+\frac{\partial \tau_{xz}}{\partial z}, \tag{2}$$

$$\frac{\partial}{\partial x}(\rho uv)+\frac{\partial}{\partial y}(\rho vv)+\frac{\partial}{\partial z}(\rho wv)=-\frac{\partial p}{\partial y}+\frac{\partial \tau_{yy}}{\partial y}+\frac{\partial \tau_{yz}}{\partial z}, \tag{3}$$

$$\frac{\partial}{\partial x}(\rho uw)+\frac{\partial}{\partial y}(\rho vw)+\frac{\partial}{\partial z}(\rho ww)=-\frac{\partial p}{\partial z}+\frac{\partial \tau_{zy}}{\partial y}+\frac{\partial \tau_{zz}}{\partial z}. \tag{4}$$

2.3. *Enthalpy*

$$\begin{aligned}\frac{\partial}{\partial x}(\rho uh)+\frac{\partial}{\partial y}(\rho vh)+\frac{\partial}{\partial z}(\rho wh)&=\frac{\partial q_y}{\partial y}+\frac{\partial q_z}{\partial z}+u\frac{\partial \bar{p}}{\partial x}+v\frac{\partial p}{\partial y}+w\frac{\partial p}{\partial z}+S_\mu\\&\quad-\int_0^\infty 4\pi(1-\omega_\nu)\beta_\nu\left(I_{b\nu}-\frac{G_\nu}{4\pi}\right)\mathrm{d}\nu.\end{aligned} \tag{5}$$

In equation (5), the integral term is the divergence of radiative heat flux, S_μ denotes the viscous dissipation of kinetic energy

$$S_\mu=\mu_{\text{eff}}\left\{2\left[\left(\frac{\partial v}{\partial y}\right)^2+\left(\frac{\partial w}{\partial z}\right)^2\right]+\left(\frac{\partial w}{\partial y}+\frac{\partial v}{\partial z}\right)^2+\left(\frac{\partial u}{\partial y}\right)^2+\left(\frac{\partial u}{\partial z}\right)^2\right\}, \tag{6}$$

and G_ν is the incident radiation

$$G_\nu=\int_{\phi=0}^{2\pi}\int_{\theta=0}^{\pi} I_\nu \sin\theta\,\mathrm{d}\theta\,\mathrm{d}\phi. \tag{7}$$

2.4. *Turbulence*

Having invoked the parabolic flow simplification, the shear stresses and heat transfer rates are expressed as

$$\tau_{xy} = (\mu_l + \mu_t)\frac{\partial u}{\partial y},$$

$$\tau_{xz} = (\mu_l + \mu_t)\frac{\partial u}{\partial z},$$

$$\tau_{yz} = \tau_{zy} = (\mu_l + \mu_t)\left(\frac{\partial v}{\partial z} + \frac{\partial w}{\partial y}\right),$$

$$\tau_{yy} = 2(\mu_l + \mu_t)\frac{\partial v}{\partial y},$$

$$\tau_{zz} = 2(\mu_l + \mu_t)\frac{\partial w}{\partial z}, \tag{8}$$

$$q_y = \left(\frac{\mu_l}{\sigma_l} + \frac{\mu_t}{\sigma_t}\right)\frac{\partial h}{\partial y},$$

$$q_z = \left(\frac{\mu_l}{\sigma_l} + \frac{\mu_t}{\sigma_t}\right)\frac{\partial h}{\partial z}. \tag{9}$$

The turbulent viscosity in the duct is represented in terms of the kinetic energy of turbulence and its dissipation rate

$$\mu_t = C_D\frac{\rho k^2}{\varepsilon}. \tag{10}$$

The two turbulence quantities, k and ε, are modeled by the following transport equations

$$\frac{\partial}{\partial x}(\rho uk) + \frac{\partial}{\partial y}(\rho vk) + \frac{\partial}{\partial z}(\rho wk) = \frac{\partial}{\partial y}\left(\frac{\mu_l}{\sigma_k}\frac{\partial k}{\partial y}\right) + \frac{\partial}{\partial z}\left(\frac{\mu_t}{\sigma_k}\frac{\partial k}{\partial z}\right) + S_k - \rho\varepsilon, \tag{11}$$

$$\frac{\partial}{\partial x}(\rho u\varepsilon) + \frac{\partial}{\partial y}(\rho v\varepsilon) + \frac{\partial}{\partial z}(\rho w\varepsilon) = \frac{\partial}{\partial y}\left(\frac{\mu_t}{\sigma_\varepsilon}\frac{\partial \varepsilon}{\partial y}\right) + \frac{\partial}{\partial z}\left(\frac{\mu_t}{\sigma_\varepsilon}\frac{\partial \varepsilon}{\partial z}\right) + \frac{C_1 S_k \varepsilon}{k} - C_2\rho\frac{\varepsilon^2}{k}, \tag{12}$$

where S_k is the rate of conversion of the mean energy into turbulence energy by the action of turbulent stresses on mean velocity gradients

$$S_k = \mu_t\left\{2\left[\left(\frac{\partial v}{\partial y}\right)^2 + \left(\frac{\partial w}{\partial z}\right)^2\right] + \left(\frac{\partial w}{\partial y} + \frac{\partial v}{\partial z}\right)^2 + \left(\frac{\partial u}{\partial y}\right)^2 + \left(\frac{\partial u}{\partial z}\right)^2\right\}. \tag{13}$$

The various terms in equation (11) for k and equation (12) for ε represent the convective transport, diffusive transport, rate of production, and rate of dissipation of the respective quantities. The full justification and interpretation of these terms are offered elsewhere [8].

2.5. *Radiation transport*

$$l_x\frac{\partial I_\nu}{\partial x} + l_y\frac{\partial I_\nu}{\partial y} + l_z\frac{\partial I_\nu}{\partial z} + \beta_\nu I_\nu = (1-\omega_\nu)\beta_\nu I_{b\nu} + \frac{\omega_\nu\beta_\nu}{4\pi}\int_{4\pi} I_\nu\,\mathrm{d}\Omega. \tag{14}$$

In equation (14), l_x, l_y and l_z are the directional cosines, and Ω is the solid angle.

$$l_x = \sin\theta\cos\phi, \tag{15}$$

$$l_y = \sin\theta\sin\phi, \tag{16}$$

$$l_z = \cos\theta, \tag{17}$$

and

$$\mathrm{d}\Omega = \sin\theta\,\mathrm{d}\theta\,\mathrm{d}\phi. \tag{18}$$

Solution of the radiation transport equation will be developed in the next section, followed by the complete solution of the combined radiation and convection problem in Section 4.

3. SOLUTION OF THE RADIATION TRANSPORT EQUATION

In this study, the moment method is used to derive the solution of the radiation transport equation. Following Ozisik [9], the method consists of representing the intensity in the form

$$I_\nu(x,y,z;l_x,l_y,l_z) = F_{0\nu}(x,y,z) + F_{1\nu}(x,y,z)l_x + F_{2\nu}(x,y,z)l_y + F_{3\nu}(x,y,z)l_z. \tag{19}$$

Integration of equation (19) over all angles shows that

$$F_{0\nu} = \frac{G_\nu}{4\pi}. \tag{20}$$

Furthermore, substituting equation (19) into equation (14), multiplying the resulting equation successively by l_x, l_y and l_z and in each case integrating over the solid angle 4π, one obtains

$$F_{1\nu} = -\frac{1}{4\pi}\frac{1}{\beta_\nu}\frac{\partial G_\nu}{\partial x} = \frac{3}{4\pi}Q_{\nu x},$$

$$F_{2\nu} = -\frac{1}{4\pi}\frac{1}{\beta_\nu}\frac{\partial G_\nu}{\partial y} = \frac{3}{4\pi}Q_{\nu y},$$

$$F_{3\nu} = -\frac{1}{4\pi}\frac{1}{\beta_\nu}\frac{\partial G_\nu}{\partial z} = \frac{3}{4\pi}Q_{\nu z}. \tag{21}$$

Finally, substituting equation (19) into equation (14), integrating the resulting equation over the solid angle 4π and making use of equations (21), the governing equation for G_ν is obtained

$$\frac{\partial}{\partial x}\left(\frac{1}{\beta_\nu}\frac{\partial G_\nu}{\partial x}\right) + \frac{\partial}{\partial y}\left(\frac{1}{\beta_\nu}\frac{\partial G_\nu}{\partial y}\right) + \frac{\partial}{\partial z}\left(\frac{1}{\beta_\nu}\frac{\partial G_\nu}{\partial z}\right) - 3(1-\omega_\nu)\beta_\nu G_\nu = -12\pi(1-\omega_\nu)\beta_\nu I_{b\nu}.$$

Neglecting axial transfer of heat, the foregoing

equation simplifies to

$$\frac{\partial}{\partial y}\left(\frac{1}{\beta_v}\frac{\partial G_v}{\partial y}\right)+\frac{\partial}{\partial z}\left(\frac{1}{\beta_v}\frac{\partial G_v}{\partial z}\right)-3(1-\omega_v)\beta_v G_v = -12\pi(1-\omega_v)\beta_v I_{bv}. \quad (22)$$

3.1. *Boundary conditions*

For a systematic derivation of the boundary conditions, equation (19) is written as

$$I_v=\frac{1}{4\pi}[G_v+3l_yQ_{vy}+3l_zQ_{vz}]. \quad (23)$$

For the diffusely reflecting wall whose outward normal is in the positive y-direction ($y = H$)

$$Q_{vy}^{-}=(1-\varepsilon_w)Q_{vy}^{+}+\pi\varepsilon_w I_{wv}, \quad (24)$$

where Q_{vy}^{-} and Q_{vy}^{+} are directional heat fluxes in the negative and positive y-directions, defined as

$$Q_{vy}^{+}=\int_{\hat{\Omega}\cdot\hat{j}>0}\hat{\Omega}\cdot\hat{j}I_v\,d\Omega, \quad (25)$$

$$Q_{vy}^{-}=\int_{\hat{\Omega}\cdot\hat{j}<0}\hat{\Omega}\cdot\hat{j}I_v\,d\Omega, \quad (26)$$

where

$$\hat{\Omega}=l_x\hat{i}+l_y\hat{j}+l_z\hat{k}.$$

Substituting equation (23) into equations (25) and (26) and performing the appropriate integrations, one obtains

$$Q_{vy}^{+}=\frac{G_v}{4}+\frac{Q_{vy}}{2}, \quad (27)$$

and

$$Q_{vy}^{-}=\frac{G_v}{4}-\frac{Q_{vy}}{2}, \quad (28)$$

so that the boundary condition (24) becomes

$$\frac{2}{3}\frac{2-\varepsilon_w}{\varepsilon_w}\frac{1}{\beta_v}\frac{\partial G_v}{\partial y}+G_v=4\pi I_{wv}, \quad y=H. \quad (29)$$

Similarly, for the diffusely reflecting wall whose normal is in the negative y-direction ($y = 0$)

$$Q_{vy}^{+}=(1-\varepsilon_w)Q_{vy}^{-}+\pi\varepsilon_w I_{wv}, \quad (30)$$

which with the use of equations (27) and (28) becomes

$$-\frac{2}{3}\frac{2-\varepsilon_w}{\varepsilon_w}\frac{1}{\beta_v}\frac{\partial G_v}{\partial y}+G_v=4\pi I_{wv}, \quad y=0. \quad (31)$$

The boundary conditions for the walls normal to the z-direction may be derived similarly; these are:

$$-\frac{2}{3}\frac{2-\varepsilon_w}{\varepsilon_w}\frac{1}{\beta_v}\frac{\partial G_v}{\partial z}+G_v=4\pi I_{wv}, \quad z=0, \quad (32)$$

$$\frac{2}{3}\frac{2-\varepsilon_w}{\varepsilon_w}\frac{1}{\beta_v}\frac{\partial G_v}{\partial z}+G_v=4\pi I_{wv}, \quad z=W. \quad (33)$$

In deriving the foregoing boundary conditions, it has been assumed that the four walls of the duct are at the same temperature, and that the origin of the coordinate system is located in a corner.

Equation (22) subject to the boundary conditions (29) and (31)–(33) constitutes a fully-defined second-order partial differential equation for G_v. Before developing its solution, we mention that within the approximation of the moment method, all the radiation quantities of interest namely, intensity, heat flux and divergence of heat flux, are given in terms of G_v. Two types of solutions are developed next; the first is a series type closed-form analytical solution, the second is numerical.

3.2. *Analytical solution*

Because of linearity, equation (22) admits a closed-form analytical solution. First, it is possible to scale the extinction coefficient out of the problem by defining optical thicknesses as

$$\tau=\int_0^y\beta_v\,dy,$$

$$\xi=\int_0^z\beta_v\,dz.$$

Then, by the method of Green's functions, the following solution is obtained

$$G_v(\tau,\xi)=4\pi I_{wv}+\int_0^{\tau_0}\int_0^{\xi_0}4\pi a_v^2(I_{bv}-I_{wv})\times K_v(\tau,\xi\,|\,\xi',\tau')\,d\xi'\,d\tau', \quad (34)$$

where K_v is the Green's function

$$K_v(\tau,\xi\,|\,\xi',\tau')=\sum_{n=0}^{\infty}A_n^2g_n(\xi\,|\,\xi')[\gamma\lambda_n\cos\lambda_n\tau+\sin\lambda_n\tau]\times[\gamma\lambda_n\cos\lambda_n\tau'+\sin\lambda_v\tau'], \quad (35)$$

$$A_n^2=\frac{2}{(1+\gamma^2\lambda_n^2)\tau_0+2\gamma}, \quad \gamma=\frac{2}{3}\frac{2-\varepsilon_w}{\varepsilon_w},$$

λ_n is the eigenvalue of the transcendental equation

$$\tan\lambda_n\tau_0=\frac{2\gamma\lambda_n}{\gamma^2\lambda_n^2-1},$$

$$g_n(\xi|\xi')=\{-\delta_v\exp[b_v(-2\xi_0+\xi')]+\exp(-b_v\xi')\}[\delta_v\exp(-\beta_v\xi)+\exp(b_v\xi)]/\alpha_v, \quad \text{for } \xi<\xi',$$

$$g_n(\xi\,|\,\xi')=[\delta_v\exp(-b_v\xi')+\exp(b_v\xi')]\times\{-\delta_v\exp[b_v(-2\xi_0+\xi)]+\exp(-b_v\xi)\}/\alpha_v, \quad \text{for } \xi>\xi',$$

$$\delta_v=(1-\gamma b_v)/(1+\gamma b_v), \quad b_v=(a_v^2+\lambda_n^2)^{1/2},$$

$$a_v=[3(1-\omega_v)]^{1/2},$$

$$\alpha_v=2b_v\delta_v[\delta_v\exp(-2b_v\xi_0)+1],$$

$$\tau_0=\int_0^H\beta_v\,dy,$$

and

$$\xi_0 = \int_0^W \beta_v \, dz.$$

3.3. *Numerical solution*

Equation (22) can be easily discretized by the method of central finite differences as

$$\frac{\partial}{\partial y}\left(\frac{1}{\beta_v}\frac{\partial G_v}{\partial y}\right)_{ij} = \frac{1}{(y_{i+1/2}-y_{i-1/2})}\left[\left(\frac{1}{\beta_v}\frac{\partial G_v}{\partial y}\right)_{i+1/2j} - \left(\frac{1}{\beta_v}\frac{\partial G_v}{\partial y}\right)_{i-1/2j}\right]$$

$$= \frac{1}{(y_{i+1/2}-y_{i-1/2})}\left[\frac{1}{\beta_{v_{i+1/2j}}}\frac{G_{v_{i+1}j}-G_{v_{ij}}}{y_{i+1}-y_i} - \frac{1}{\beta_{v_{i-1/2j}}}\frac{G_{v_{ij}}-G_{v_{i-1}j}}{y_i-y_{i-1}}\right],$$

$$\frac{\partial}{\partial z}\left(\frac{1}{\beta_v}\frac{\partial G_v}{\partial z}\right)_{ij} = \frac{1}{(z_{j+1/2}-z_{j-1/2})}\left[\left(\frac{1}{\beta_v}\frac{\partial G_v}{\partial z}\right)_{ij+1/2} - \left(\frac{1}{\beta_v}\frac{\partial G_v}{\partial z}\right)_{ij-1/2}\right]$$

$$= \frac{1}{(z_{j+1/2}-z_{j-1/2})}\left[\frac{1}{\beta_{v_{ij+1/2}}}\frac{G_{v_{ij+1}}-G_{v_{ij}}}{z_{j+1}-z_j} - \frac{1}{\beta_{v_{ij-1/2}}}\frac{G_{v_{ij}}-G_{v_{ij-1}}}{z_j-z_{j-1}}\right].$$

On collecting the coefficients of the discretized equation, the following finite difference equation is obtained

$$A_{ij}G_{v_{ij}} = B_{ij}G_{v_{i+1}j} + C_{ij}G_{v_{i-1}j} + D_{ij}G_{v_{ij+1}} + E_{ij}G_{v_{ij-1}} + F_{ij}, \quad (36)$$

where

$$B_{ij} = \frac{1}{\beta_{v_{i+1/2j}}}\frac{1}{(y_{i+1/2}-y_{i-1/2})(y_{i+1}-y_i)},$$

$$C_{ij} = \frac{1}{\beta_{v_{i-1/2j}}}\frac{1}{(y_{i+1/2}-y_{i-1/2})(y_i-y_{i-1})},$$

$$D_{ij} = \frac{1}{\beta_{v_{ij+1/2}}}\frac{1}{(z_{j+1/2}-z_{j-1/2})(z_{j+1}-z_j)},$$

$$E_{ij} = \frac{1}{\beta_{v_{ij-1/2}}}\frac{1}{(z_{j+1/2}-z_{j-1/2})(z_j-z_{j-1})},$$

$$A_{ij} = B_{ij}+C_{ij}+D_{ij}+E_{ij}+3(1-\omega_{v_{ij}})\beta_{v_{ij}},$$

and

$$F_{ij} = 12\pi(1-\omega_{v_{ij}})\beta_{v_{ij}}I_{bv_{ij}}.$$

The boundary conditions [equations (29), (30), (32) and (33)], have been discretized through forward differencing for the two walls adjacent to the origin and through backward differencing for the other two walls. The resulting finite-difference equations bear the same form as equation (36). The complete set of finite-difference equations is solved by an iterative line-by-line elimination procedure, called the tridiagonal matrix inversion algorithm (TDMI). In this procedure, the set of algebraic equations is solved alternately along lines of constant y and constant z. When a line of constant y is solved, the contributions from adjacent constant y lines is added to F_{ij}, thus reducing the equations set to the tridiagonal form, which is easily solved by Gauss elimination procedure. A similar procedure is repeated when solving lines of constant z. Alternate y and z sweeps are performed until the residuals are reduced to acceptable values.

3.4. *Comparison of methods*

TDMI has proven to be a rather slow matrix inversion algorithm for the radiation problem. As many as 1000 sweeps were required to achieve acceptable convergence. The convergence criterion has been established in terms of the following heat balance equation

$$\int\int\int 4\pi(1-\omega_v)\beta_v\left(I_{bv}-\frac{G_v}{4\pi}\right)dy\,dz\,dv = \int\int \mathbf{Q}_{vw}\cdot\mathbf{n}\,dS\,dv,$$

where S is the perimeter of the duct. The foregoing equation merely states that the volumetric cooling rate of the gas should equal the radiative heat transfer to the walls of the duct. The slow convergence of TDMI is attributed to two reasons: (1) the lack of a good initial guess; and (2) the boundary conditions are neither Dirichlet nor Neumann type but instead are of a mixed type. Other algorithms are presently being investigated that may be more efficient than TDMI. One candidate algorithm that looks particularly promising is the conjugate gradient method.

Unfortunately, the analytical method has proven to be even slower. The slow computation speed is a consequence of the Green's function of equation (35) having a series form and the required double integration in equation (34) for calculating G_v. For this reason, the analytical method has been abandoned in favor of the numerical solution.

4. COMPLETE NUMERICAL SOLUTION

Solution of the fluid equations is based on the recommendations of Patankar and Spalding [10]. The fluid equations are finite-differenced by integrating the differential equations over the control volumes surrounding the locations of the flow variables. All flow variables except v and w are stored at the grid nodes. The storage for the velocity component v is staggered in the y-direction, being stored between the grid points. Similarly, storage for the w component is staggered in the z-direction. The convective fluxes in fluid equations

are discretized by the upwinding technique and the diffusional fluxes by central differencing. The resulting finite-difference equations bear the form of equation (36) and are solved by the TDMI algorithm. Being parabolic, the marching scheme is employed to advance the solution of fluid equations from the inlet to the exit of the duct. At each successive cross-sectional plane, all the variables are solved for, in the following sequence.

(a) First, the radiation transport equation is solved for G_v and, hence, the heat flux and the divergence of radiative heat flux.

(b) The equations for enthalpy, kinetic energy of turbulence and its dissipation rate are solved.

(c) New fluid properties are evaluated from updated enthalpy and pressure at the previous axial location.

(d) The momentum equations are solved using the pressure field at the previous axial location.

(e) The velocities calculated in step (d) may not satisfy the continuity equation. Therefore, the pressure field is corrected such that the implied velocities would obey the continuity equation. The satisfaction of the integral continuity over the cross-sectional plane gives the correction to $d\bar{p}/dx$ and hence the u field; and the satisfaction of the mass continuity at each grid point gives the corrections to the pressure field p and hence the velocity components v and w.

4.1. *Further details*

The normally encountered difficulty in resolving the turbulent flow field in near-wall regions is alleviated by using wall functions. The radiation term in the energy equation (5) is treated as a source term and evaluated for temperature distribution prevailing at the preceding axial location. The spectral integration is effected by first dividing the radiation wave band (200–15 000 cm^{-1}) into seven bands. Over each of these bands, a 16 point Gauss quadrature scheme is used for performing integrations. Thus, in all equation (22) needs to be solved 112 times (at every axial location), once for each frequency being considered. Given the slow convergence rate of the finite-difference equations for G_v, it becomes imperative to seek some means of speeding up the computations. A simple recourse for accomplishing this objective consists of not updating the radiation solution at every marching step. Some numerical experimentation was conducted to determine how infrequently the radiation terms can be updated without incurring an unacceptable loss in accuracy, defined as 5% inaccuracy in heat flux. On the basis of this experimentation, radiation terms were updated once every 50 cm. Additional details are available in refs. [1–3].

4.2. *Radiation properties*

In this study, carbon dioxide, water vapor and particles are considered to be the major species participating in thermal radiation. For carbon dioxide and water vapor, the spectral absorption coefficients are calculated from the band model [11]. The correlations used in this model include the contributions from all five bands in carbon dioxide and four bands in water vapor, and the pressure broadening effect. For particles, the spectral absorption and scattering coefficients are calculated from the Mie theory. For distributed size particles considered, these are computed by integrating over the particle size the product of the projected area of the particles, efficiency factors for absorption or scattering, and particle size distribution function.

5. RESULTS AND DISCUSSION

Sample calculations have been performed for flow in a square duct, 0.5×0.5 m in cross section and 5 m in length. Additional data used in the calculations are: mass flow rate of the gas = 7.50 kg s^{-1}, inlet temperature = 2400 K, wall temperature = 1000 K, inlet thermal and velocity boundary layer thickness = 5 cm, inlet pressure = 1 atm, mole fraction of carbon dioxide = 0.15, and mole fraction of water vapor = 0.15. The equation of state of the products of coal combustion is used in the calculations [1]. The assumed particle size spectrum is listed in Table 1. The data of Foster and Howarth [12], valid for coal particles, are used to determine the complex refractive index of particles. Accordingly

$$m = 0.35 - i(1.6) \quad \text{for } \lambda < 6\ \mu\text{m},$$

$$m = 0.35 + 0.733(\lambda - 6) - i[1.6 + 0.125(\lambda - 6)] \quad \text{for } \lambda > 6\ \mu\text{m}.$$

It is assumed that throughout the flow field, the particles are uniformly distributed and that the mole fractions of carbon dioxide and water vapor remain unchanged. In order to understand the nature of radiative heat transfer and its interaction with convection and the velocity flow field, a parametric study is conducted by varying the concentration of the participating species from the above-stated values.

Figure 1 shows the peripheral variation of radiative heat flux normalized with respect to σT_0^4, where T_0 is a reference temperature arbitrarily assigned to the wall value. Because of symmetry, the variation is shown along one wall only. Also listed in Fig. 1 is the axial variation of centerline temperature. At $x/H = 1$, there is a distinct peak in radiative heat flux at the center of

Table 1. Particle size spectrum

Size, μm	0.015	0.03	0.06	0.14	0.35	0.72	5.0	4.0
Number density, cm^{-3}	7×10^1	7×10^3	2×10^3	3×10^7	1.5×10^3	7×10^2	2×10^2	7×10^2

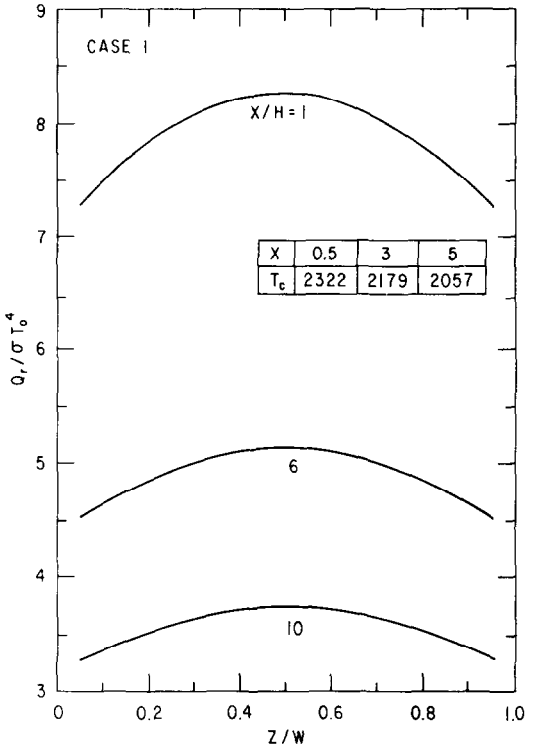

FIG. 1. Peripheral variation of radiative heat flux.

the wall. The presence of the peak is attributed to enhanced absorption of radiation in the low-temperature corner region reducing the local heat flux in that region. As the flow progresses further, the radiative heat flux is observed to diminish in response to the cooling of the gas. However, its peripheral variation is identical to that at $x/H = 1$.

For the conditions of Fig. 1, the peripheral variation of convective heat flux at three locations is plotted in Fig. 2. As in the radiation mode, the convective heat flux is seen to be higher in the center than the corner. This is different from the radiation mode, however, in that there is no peak in convective heat flux at $x/H = 1$. Instead, away from the corner boundary layer, there is a plateau, emphasizing the different natures of the radiation (a volumetric process) and convection (a surface phenomenon) modes of heat transfer. Further downstream, the boundary layer grows causing a drop in convective heat flux; and the corner boundary layers merge and engulf the complete flow, so that at $x/H = 10$ the plateau in convective heat flux, seen earlier, vanishes.

In order to investigate the interaction between convection and radiation and to evaluate the contribution of individual participating species to radiative heat transfer, a parametric study is conducted next with the calculations of Figs. 1 and 2 (called case 1) providing the datum. Three additional calculations are performed. In the first (case 2), only carbon dioxide and water vapor (no particles) are considered to be the participating species; in cases 3 and 4 carbon dioxide (no particles, no water vapor) and water vapor (no particles, no carbon dioxide) are respectively considered as the sole participating species. For these four cases, the peripheral variation of radiative heat flux, normalized by σT_0^4, at $x/H = 10$ is plotted in Fig. 3. The difference between curves 1 and 2 is indicative of the contribution of particles to radiative heat transfer; the contribution of particles is observed to be nearly 66% of the total. Comparing curves 3 and 4, carbon dioxide contribution is approximately 50% greater than that of water vapor. Again comparing curve 2 with curves 3 and 4, the simultaneous contribution to heat transfer of carbon dioxide and water vapor is less than the sum of the individual contributions. This is because of the

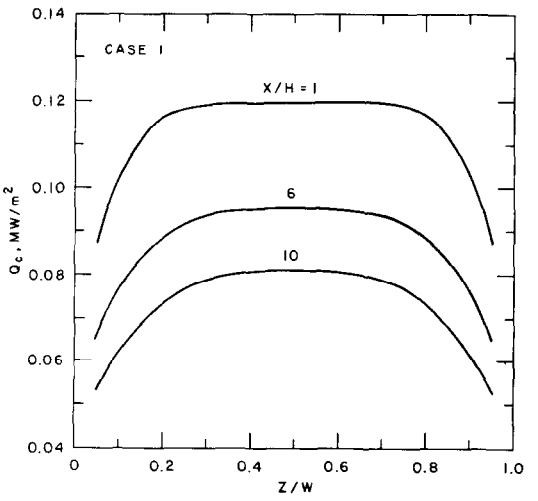

FIG. 2. Peripheral variation of convective heat flux.

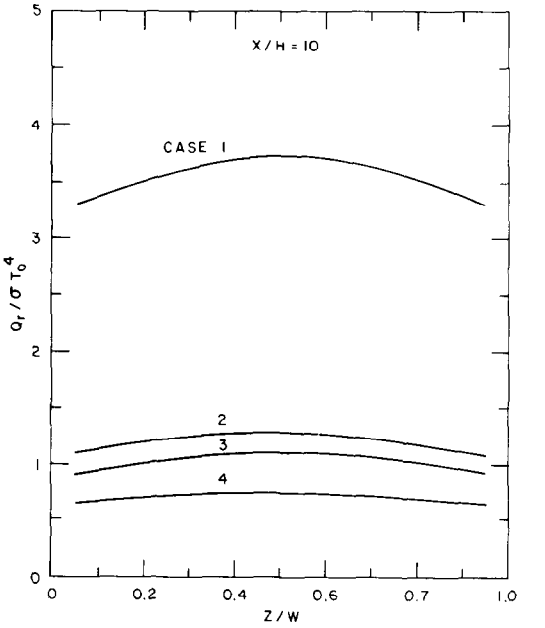

FIG. 3. Peripheral variation of radiative heat flux for different gas compositions.

Table 2. Extinction coefficient and scattering albedo

ν (cm^{-1})	Case 1 β_ν (m^{-1})	Case 1 ω_ν	Case 2 β_ν (m^{-1})	Case 2 ω_ν	Case 3 β_ν (m^{-1})	Case 3 ω_ν	Case 4 β_ν (m^{-1})	Case 4 ω_ν
200	0.053	0.159	0.015	0.0	0.006	0.0	0.009	0.0
500	0.798	0.071	0.626	0.0	0.620	0.0	0.030	0.0
800	0.887	0.061	0.663	0.0	0.611	0.0	0.076	0.0
1450	0.704	0.071	0.440	0.0	0.0	0.0	0.461	0.0
2100	1.152	0.041	0.853	0.0	0.691	0.0	0.180	0.0
2450	3.274	0.015	2.936	0.0	3.002	0.0	0.075	0.0
2800	0.453	0.112	0.081	0.0	0.019	0.0	0.064	0.0
3900	0.735	0.084	0.225	0.0	0.196	0.0	0.233	0.0
5000	0.688	0.121	0.038	0.0	0.0	0.0	0.038	0.0
5400	0.778	0.125	0.057	0.0	0.0	0.0	0.058	0.0
5800	0.798	0.140	0.014	0.0	0.0	0.0	0.014	0.0
6300	0.890	0.157	0.003	0.0	0.0	0.0	0.004	0.0
6800	1.009	0.170	0.019	0.0	0.0	0.0	0.019	0.0
10 900	2.353	0.344	0.0	0.0	0.0	0.0	0.0	0.0
15 000	3.779	0.429	0.0	0.0	0.0	0.0	0.0	0.0

overlap of the 2.7 μm bands of carbon dioxide and water vapor. Moreover, with the simultaneous participation of the two gases, the gas temperature drops faster than if they were present alone so that the combined radiative heat transfer rate is smaller than the sum of the individual rates. For the four cases studied, the extinction coefficient and scattering albedo for selected frequencies at a temperature of 2400 K are listed in Table 2.

The peripheral variation of convective heat flux for the four cases at $x/H = 10$ is depicted in Fig. 4. Of the four cases studied, the magnitude of convective heat flux for case 1 is seen to be the smallest and of case 4 the largest. This trend is opposite to that observed in Fig. 3 for radiative heat flux, and can be explained by recognizing that the larger the radiative heat flux, the lower the gas temperature and, hence, the smaller is the convective heat flux. A secondary contributory factor is that as the radiative heat flux increases, so does the thermal boundary layer thickness which leads to diminution in convective heat flux.

The effect of radiation on the growth of the thermal boundary layer is observed more clearly in Fig. 5 where the temperature profiles at $x/H = 10$ and $y/H = 0.50$ for the four cases have been plotted. In Fig. 5, temperature has been non-dimensionalized with respect to the inlet temperature rather than the centerline temperature in order to indicate the temperature level. It is observed here that whereas the boundary layers have merged for case 1 (largest radiative heat transfer), a plateau in temperature profile is still visible for case 4 (smallest radiative heat transfer). The level of temperature is consistent with the total heat transfer rate.

The axial variation of convective and radiative heat flux for the four cases is shown in Fig. 6. It is seen that in

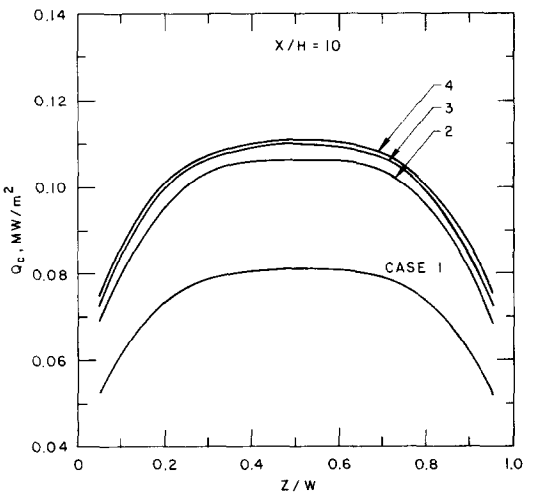

FIG. 4. Peripheral variation of convective heat flux for different gas compositions.

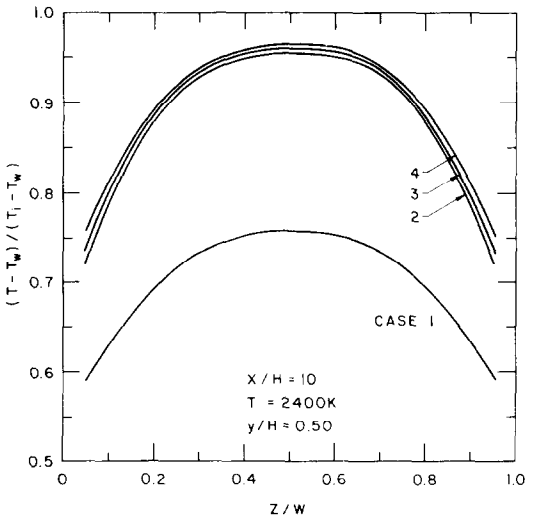

FIG. 5. Influence of radiation on temperature profile.

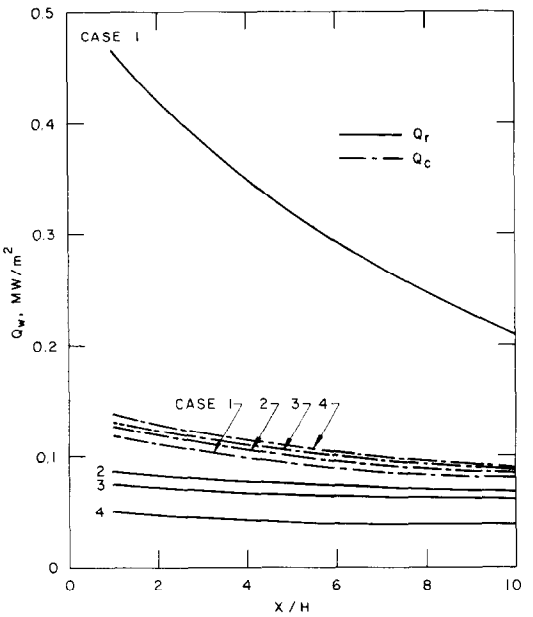

FIG. 6. Axial variation of convective and radiative heat flux.

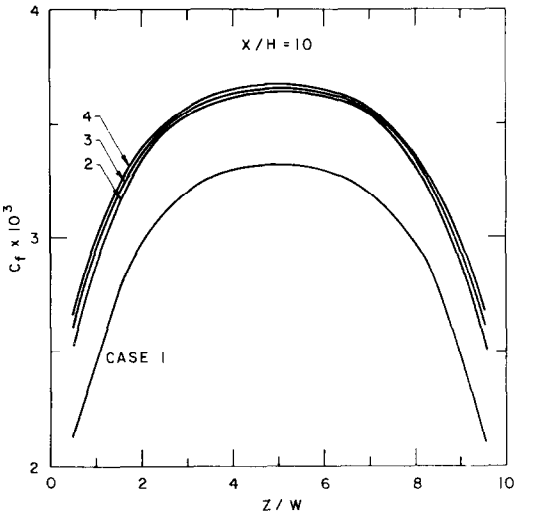

FIG. 8. Peripheral variation of friction coefficient.

case 1 the radiative heat flux diminishes rapidly along the flow direction in response to the accelerated cooling of the gas associated with the high heat transfer rate. In other cases, the decrease of radiative heat flux along the flow direction is more gradual. For the conditions of case 1 (particles present) radiation is seen to dominate over convection as the principal heat transfer mechanism. At the upstream end, radiative heat flux is greater than the convective by a factor of four, which decreases to two at the downstream end. For the conditions represented in other cases (no particles), the heat transfer by convection is larger than that by radiation but the two are comparable in magnitude.

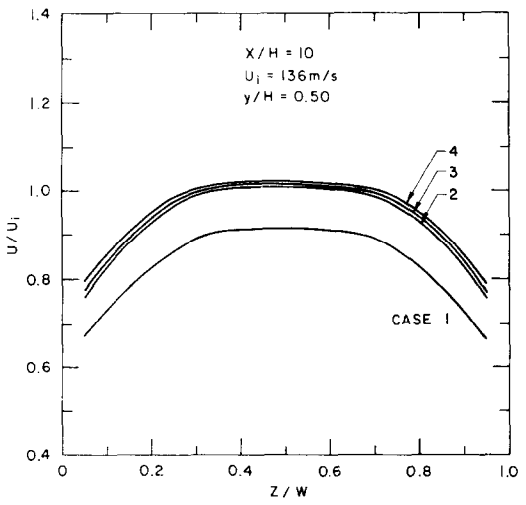

FIG. 7. Influence of radiation on velocity profile.

The effects of radiation on the velocity field are displayed in Fig. 7. Here the velocity profiles in the z-direction at $y/H = 0.50$ and $x/H = 10$ have been plotted for the four cases. The local velocity in Fig. 7 has been non-dimensionalized with respect to the inlet velocity. On comparing Figs. 5 and 7, it is observed that in the presence of thermal radiation the momentum and thermal boundary layer characteristics are quite different. In particular, for case 1 whereas the thermal boundary layer at $x/H = 10$ is fully-developed, the momentum boundary layer is not. This is because thermal radiation is a volumetric process, so that unlike convection the divergence of radiant heat flux is non-zero everywhere—even outside the boundary layer; and it has a variation throughout the flow field. Thus, the growth of the thermal boundary layer is enhanced in the presence of radiation; there is no equivalent phenomenon for the momentum boundary layer. Another indirect effect of thermal radiation seen in Fig. 7 is that the higher the radiative heat transfer, the lower the gas temperature (throughout the flow field), the greater the gas density and, therefore, the slower the flow velocity (from the continuity requirement).

Finally the effect of thermal radiation on skin friction for compressible flow is shown in Figs. 8 and 9. The only manner in which thermal radiation influences the flow field and skin friction is through fluid compressibility since in most engineering problems the radiation pressure is extremely small; for incompressible flow, no effect of thermal radiation on skin friction is anticipated. For the four cases studied, the peripheral variation of the skin-friction coefficient at $x/H = 10$ is depicted in Fig. 8. As expected, the friction coefficient is a minimum at the corner and a maximum at the midpoint of the wall. For case 1, there is approximately a 10% reduction in friction coefficient due to thermal radiation. The axial variation of the average skin-friction coefficient for the four cases is shown in Fig. 9. As expected, the effect of thermal radiation on skin

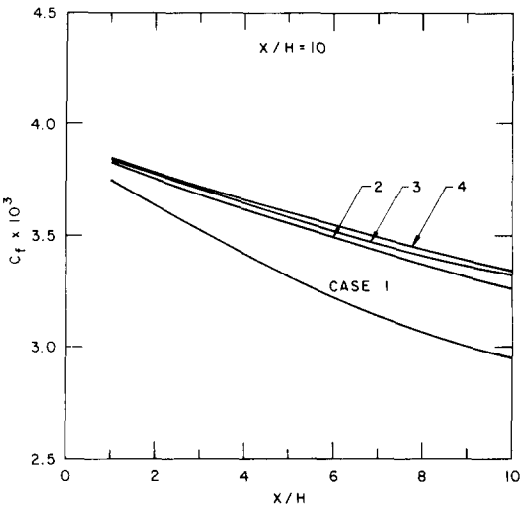

FIG. 9. Axial variation of average friction coefficient.

friction is cumulative in that the deviation of skin friction between the four cases is amplified with flow distance.

6. CONCLUSIONS

A combined convective and radiative heat transfer model for compressible, turbulent and developing flow in rectangular ducts has been formulated and solved numerically. In solving the fluid equations the assumption of parabolic flow has been invoked. The solutions of the radiation transport equation is based on the moment method. Sample calculations have been performed with carbon dioxide, water vapor, and absorbing and scattering particles considered as the species participating in thermal radiation. Based on the analysis and the sample calculations, the following conclusions can be drawn.

(1) The method of finite differences is superior to the analytical method in solving the incident radiation equation. Although used in this study, the line by line iterative technique (called TDMI algorithm) of inverting the algebraic equations, obtained from discretization of the incident radiation equation, has very slow convergence. Up to 1000 iterations were required to achieve the target convergence criterion. However, the TDMI algorithm has proved efficient in solving the discretized fluid equations. The slow convergence of TDMI in handling the radiation equations has been ascribed to: (a) lack of a good initial guess for the incident radiation field, and (b) the boundary conditions are neither of the Neumann nor Dirichlet type but are of a mixed type. As a future endeavor, the conjugate gradient method of inverting the matrix appears promising.

(2) In the sample calculations, physical differences between the convection and radiation mechanisms have been identified. Because the thermal radiation transport is a volumetric process, the divergence of radiant heat flux is non-zero everywhere in the flow field. Consequently, the peripheral variation of the radiant heat flux is continuous and shows a peak at the midpoint of the wall. On the other hand, convection is a surface phenomenon so that the divergence of convective heat flux is zero outside the thermal boundary layer (no temperature gradient). Therefore, along the periphery of a wall, the convective heat flux increases from the corner to the edge of the corner boundary layer and becomes a constant thereafter.

(3) The sample calculations show an interaction between the convection and radiation modes of heat transfer. The observed influence of radiation has been the diminution in convective heat flux. This has been explained on the basis of enhanced growth rate of the thermal boundary layer due to radiation and the general reduction in gas temperature.

(4) It has been observed that the combined contribution of carbon dioxide and water vapor to radiative heat transfer is less than the sum of individual contributions of carbon dioxide and water vapor when present alone. This is ascribed to the overlap between the 2.7 μm bands of carbon dioxide and water vapor, and to the faster cooling of gas when the two participating species are present simultaneously.

(5) The effects of thermal radiation on the velocity field and skin friction have been evaluated. The only manner in which thermal radiation affects the velocity field is through fluid compressibility since the radiation pressure is negligibly small in most engineering applications. It is observed that radiation causes the thermal boundary layer to become thicker than the momentum boundary layer. With radiative heat transfer, the gas temperature decreases, the gas density increases and, therefore, from the continuity requirement the flow velocity slows down. Finally, in the sample calculations the skin-friction coefficient was found to decrease by 10% due to thermal radiation.

REFERENCES

1. K. H. Im and R. K. Ahluwalia, Heat and mass transfer in MHD channels, *J. Energy* **5**(1), 119–125 (1981).
2. R. K. Ahluwalia and K. H. Im, Combined conduction, convection, gas radiation and particle radiation in MHD diffusers, *Int. J. Heat Mass Transfer* **24**, 1421–1430 (1981).
3. K. H. Im and R. K. Ahluwalia, Convective and radiative heat transfer in MHD radiant boilers, *J. Energy* **5**(5), 308–314 (1981).
4. M. Krook, On the solution of equation of transfer—I, *Astrophys. Jl* **122**, 488–497 (1955).
5. P. Cheng, Exact solutions and differential approximation for multi-dimensional radiative transfer in Cartesian coordinate configuration, *Prog. Astronaut. Aeronaut.* **31**, 269–308 (1972).
6. A. C. Ratzel and J. R. Howell, Two-dimensional radiation in absorbing-emitting-scattering media using the $P-N$ approximation, 82-HT-19, AIAA/ASME Fluid, Plasma, Thermophysics, and Heat Transfer Conference, St. Louis, Missouri (1982).

7. M. F. Modest, Radiative equilibrium in a rectangular enclosure bounded by gray walls, *J. Spectrosc. Radiat. Transfer* **15,** 445–461 (1975).
8. B. E. Launder and D. B. Spalding, The numerical computation of turbulent flows, *Comput. Meth. Appl. Mech. Engng* **3,** 269–289 (1974).
9. M. N. Ozisik, *Radiative Transfer*, p. 343. Wiley, New York (1973).
10. S. V. Patankar and D. B. Spalding, A calculation procedure for heat, mass and momentum transfer in three-dimensional parabolic flows, *Int. J. Heat Mass Transfer* **15,** 1787–1806 (1972).
11. C. T. Tien, Thermal radiation properties of gases, *Adv. Heat Transfer* **5,** 253–324 (1968).
12. P. J. Foster and C. R. Howarth, Optical constants of carbon and coal in the infrared, *Carbon* **6,** 719–729 (1968).

CONVECTION COMBINEE AU RAYONNEMENT DANS DES CANAUX RECTANGULAIRES

Résumé—Le transfert thermique par convection et rayonnement couplés est analysé en résolvant simultanément les équations du mouvement du fluide et l'équation du transfert radiatif. Les approximations principales sont l'hypothèse d'une équation parabolique pour le mouvement et l'utilisation de la méthode du moment pour simplifier l'équation du transfert radiatif. L'analyse est applicable à l'écoulement général turbulent d'un fluide compressible et rayonnant qui se développe dans des canaux rectangulaires en présence de particules qui diffusent. Dans les calculs, la théorie de Mie est utilisée pour déterminer les coefficients d'absorption et de diffusion des particules.

DAS ZUSAMMENWIRKEN VON KONVEKTION UND STRAHLUNG IN RECHTWINKLIGEN KANÄLEN

Zusammenfassung—Der kombinierte Wärmeaustausch durch Konvektion und Strahlung in rechtwinkligen Kanälen wird durch gleichzeitiges Lösen der Strömungsgleichungen und der Strahlungstransportgleichung untersucht. Die Hauptvoraussetzungen der Berechnung sind die Annahme eines parabolischen Profils für die Strömung und die Anwendung der Momentmethode zur Vereinfachung der Strahlungstransportgleichung. Die Berechnung ist allgemein für kompressible, turbulente, nicht voll ausgebildete Strömung strahlender Medien in rechtwinkligen Kanälen mit streuenden Partikeln anwendbar. In den Berechnungsbeispielen wird die Theorie von Mie zur Bestimmung der spektralen Absorption und der Streuungskoeffizienten der Partikel verwendet.

СМЕШАННЫЕ КОНВЕКЦИЯ И ИЗЛУЧЕНИЕ В ПРЯМОУГОЛЬНЫХ КАНАЛАХ

Аннотация—Смешанный, конвективный и лучистый, теплоперенос в прямоугольных каналах анализируется путем одновременного решения уравнений гидродинамики и уравнения лучистого переноса. Основными аппроксимациями, используемыми в анализе, являются допущение параболического течения для гидродинамических уравнений и использование метода моментов для упрощения уравнения лучистого переноса. Анализ справедлив для сжимаемого турбулентного развивающегося излучающего потока в прямоугольных каналах при наличии рассеивающих частиц. В пробных решениях используется теория Ми с целью определения коэффициентов спектрального поглощения и рассеивания на частицах.